LETTERS
PUBLISHED ONLINE: 16 MARCH 2015 | DOI: 10.1038/NGEO2388
nature geoscience

Ocean access to a cavity beneath Totten Glacier in East Antarctica

J. S. Greenbaum[1]*, D. D. Blankenship[1], D. A. Young[1], T. G. Richter[1], J. L. Roberts[2,3], A. R. A. Aitken[4], B. Legresy[2,5,6], D. M. Schroeder[7], R. C. Warner[2,3], T. D. van Ommen[2,3] and M. J. Siegert[8]

Totten Glacier, the primary outlet of the Aurora Subglacial Basin, has the largest thinning rate in East Antarctica[1,2]. Thinning may be driven by enhanced basal melting due to ocean processes[3], modulated by polynya activity[4,5]. Warm modified Circumpolar Deep Water, which has been linked to glacier retreat in West Antarctica[6], has been observed in summer and winter on the nearby continental shelf beneath 400 to 500 m of cool Antarctic Surface Water[7,8]. Here we derive the bathymetry of the sea floor in the region from gravity[9] and magnetics[10] data as well as ice-thickness measurements[11]. We identify entrances to the ice-shelf cavity below depths of 400 to 500 m that could allow intrusions of warm water if the vertical structure of inflow is similar to nearby observations. Radar sounding reveals a previously unknown inland trough that connects the main ice-shelf cavity to the ocean. If thinning trends continue, a larger water body over the trough could potentially allow more warm water into the cavity, which may, eventually, lead to destabilization of the low-lying region between Totten Glacier and the similarly deep glacier flowing into the Reynolds Trough. We estimate that at least 3.5 m of eustatic sea level potential drains through Totten Glacier, so coastal processes in this area could have global consequences.

The Totten Glacier drains into the Sabrina Coast in an area where we find coastal ice grounded below sea level and the potential for local marine ice sheet instability[12] upstream of the grounding line (Fig. 1b). We infer the bathymetry seaward of the grounding line using inversions of gravity data[9] informed by magnetics data[10] and ice-thickness measurements[11]. The inversion reveals the southwest area of the Totten Glacier Ice Shelf (TGIS) cavity is the deepest, reaching 2.7 ± 0.19 km below sea level (Fig. 2), comparable to the grounding line depths of Amery Ice Shelf[13] and the segment of the Moscow University Ice Shelf (MUIS) overlying the Reynolds Trough[11]. The shallowest area of the cavity (~300 mbsl) is found beneath the calving front of the ice shelf where a large coast-parallel ridge connects Law Dome with a peninsula of grounded ice protruding from the east side of the cavity (Fig. 2). The ridge extends 40 km seaward of the calving front and would have been a source of backstress on the Totten Glacier as recently as 1996 when ice rises were last detected[14]. The inversion reveals depressions located near the centre of the ridge (650 ± 190 mbsl) and to the east of the grounded ice peninsula (860 ± 190 mbsl) (Fig. 2, Profile A–A′). Looking along the long axis of the full Totten cavity we see it is an average of 500 m deeper along the western (Law Dome) side. We infer two basins on the long axis reaching depths of 2.7 ± 0.19 km and 2.0 ± 0.19 km (SW and NE, respectively; Fig. 2) separated by a narrow ridge causing an ice rise near the middle of the ice shelf (the left-hand panel in Fig. 2)[14].

Published grounding lines[14,15] indicate an area of grounded ice bounded by the MUIS to the north and an eastward extension of the TGIS to the south (Fig. 3). We use hydrostatic calculations and basal reflection and specularity analyses from radar data to show that a subglacial oceanic trough connects through this zone beneath nearly 1,000 m of floating ice. We identify floating ice by comparing the observed ice-surface elevation to that computed from concurrently measured ice thickness assuming hydrostatic equilibrium[16] (Fig. 3). The hydrostatic criterion is sensitive to an uncertain firn model[17] so we analyse five lines to investigate where ice is floating; two lines crossing the trough acquired one year apart (Profiles C and D) and lines on either side, sampling areas known to be floating, where the firn is likely to be similar. Line segments sampling the trough (red points) and nearby areas known to be floating (yellow, orange, and cyan) lie along the hydrostatic line (Fig. 3a), indicating that the modelled firn thickness is acceptable for this area and that the ice over the channel is also floating. Profiles A and B reveal floatation westward of the published grounding line. The area of the trough that we find to be in hydrostatic equilibrium corresponds to where a radar satellite image[18] suggests steep slopes bounding an ice-surface depression (transparent overlay in Figs 2 and 3).

The width of the trough would be just over 4 km if it were defined by hydrostatic criteria alone. However, the true grounding line is often landward of the hydrostatic point owing to rigidity in floating ice; so, other techniques must be used to infer the extent of subglacial water. Profile D–D′ in Fig. 3 illustrates that the basal reflectivity over the trough is 10 to 15 dB higher than on either side. Established radar literature demonstrates the relative reflected power of seawater and unfrozen bedrock is ~12 dB (refs 19–21), providing confidence in our interpretation that the ice over the trough floats on seawater. This is consistent with the bright region beginning near easting 2,245 km in the radargram included in Fig. 3. Taking the area of elevated reflectivity to represent water between the true grounding line and where the ice is in full hydrostatic equilibrium, we find that the trough is closer to 4.9 km across.

We investigate the character of the ice–water interface over the trough using the specularity of the basal radar returns[22] along Profile D–D′. The proportion of specular to diffuse energy in radar bed echoes is used to identify subglacial water[22] because melt processes

[1]Institute for Geophysics, University of Texas at Austin, Austin, Texas 78758, USA. [2]Antarctic Climate & Ecosystems Cooperative Research Centre, University of Tasmania, Private Bag 80, Hobart, Tasmania 7001, Australia. [3]Australian Antarctic Division, Channel Highway, Kingston, Tasmania 7050, Australia. [4]School of Earth and Environment, The University of Western Australia, Perth, Western Australia 6009, Australia. [5]CSIRO Oceans and Atmosphere Flagship, Castray Esplanade, Hobart, Tasmania 7000, Australia. [6]CNRS-LEGOS, 14 Av. E. Belin, 31400, Toulouse, France. [7]Jet Propulsion Laboratory, California Institute of Technology, Pasadena, California 91109, USA. [8]Grantham Institute and Department of Earth Sciences and Engineering, Imperial College London, London SW7 2AZ, UK. *e-mail: jamin@utexas.edu

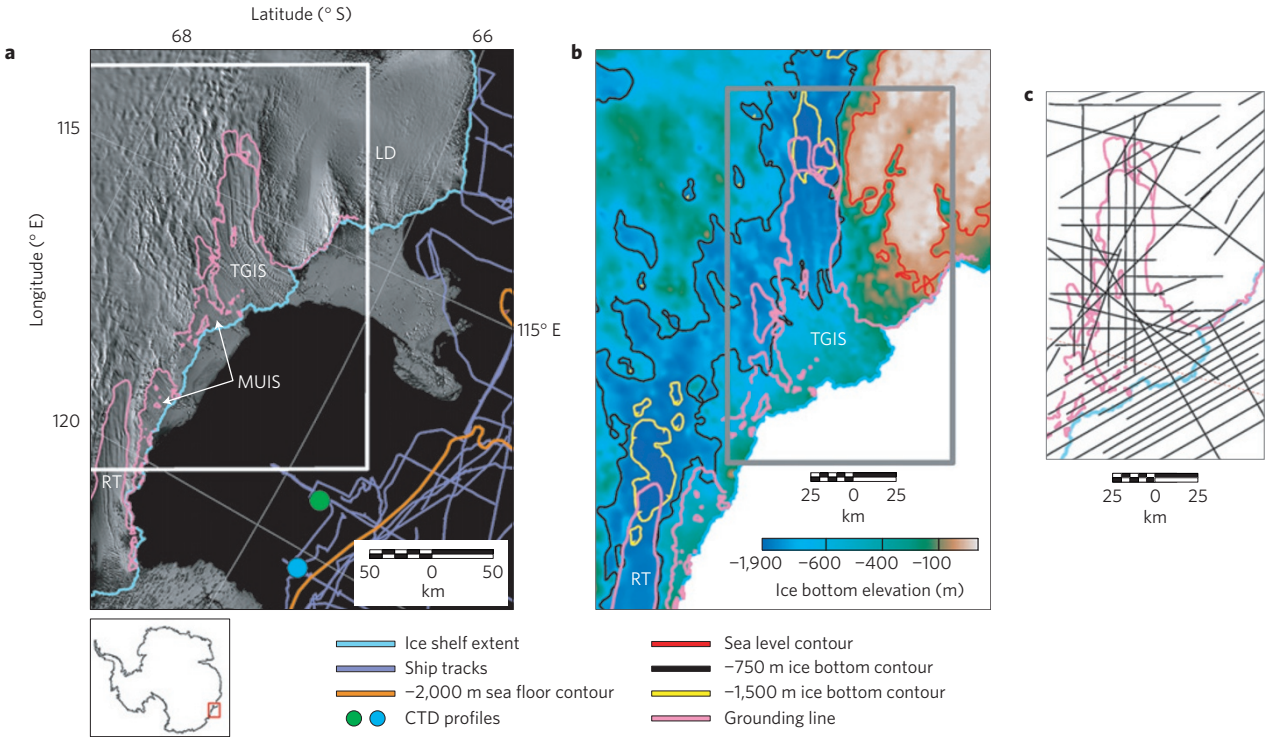

Figure 1 | Satellite imagery, a priori ice-bottom elevation map, and gravity data coverage of the study area. a, The Sabrina Coast with the Totten Glacier Ice Shelf (TGIS), Moscow University Ice Shelf (MUIS), Law Dome (LD) and the Reynolds Trough (RT) labelled over the MODIS-derived Mosaic of Antarctica (MOA; ref. 18). Coloured lines and marks denote the nearest available ship tracks with sea floor observations, the grounding line from data acquired in 1996 (ref. 14), ice-shelf extent[15], −2,000 m sea floor contour[26], and published conductivity–temperature–depth (CTD) profiles[7]. **b**, Ice-bottom elevation derived from ice-sounding radar identifying a low-lying area between the TGIS and RT in the region indicated by the white box in **a**. **c**, Airborne gravity lines (black) used in the 3D inversion which was computed within the grey box outlined in **b**.

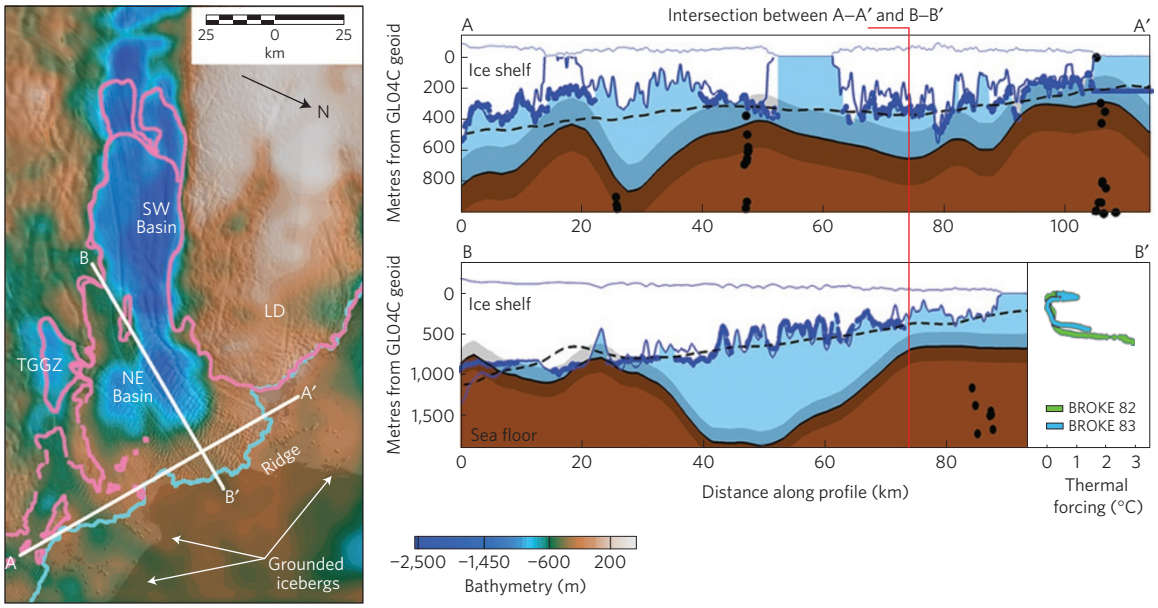

Figure 2 | Shape of the sea floor beneath the Totten Glacier Ice Shelf. Left-hand panel: The TGIS bathymetry is plotted with the MOA (ref. 18) (partially transparent), map area is the same as Fig. 1c. A basement ridge, major basins, grounded icebergs (Supplementary Movies) and the eastern Totten Glacier Grounding Zone (TGGZ) are labelled for reference. Profile A–A′ crosses the major oceanic entryways. Profile B–B′ crosses a major ice rise, the NE Basin and the basement ridge; thermal forcing computed from published CTD profiles from the BROKE expedition (ref. 7; locations shown in Fig. 1) is plotted using the same vertical scale. Laser-derived ice-surface elevation (thin blue line), ice-bottom elevation from radar sounding (where available; thick blue points), and ice-bottom elevation computed from the surface elevation assuming floatation (medium blue line) are plotted above the inverted sea floor (brown). Grey shading in both profiles represents the estimated root mean square error between inverted and measured depths. Depth to magnetic basement solutions (black points) and the Bedmap 2 sea floor[26] (dashed black line) are also plotted.

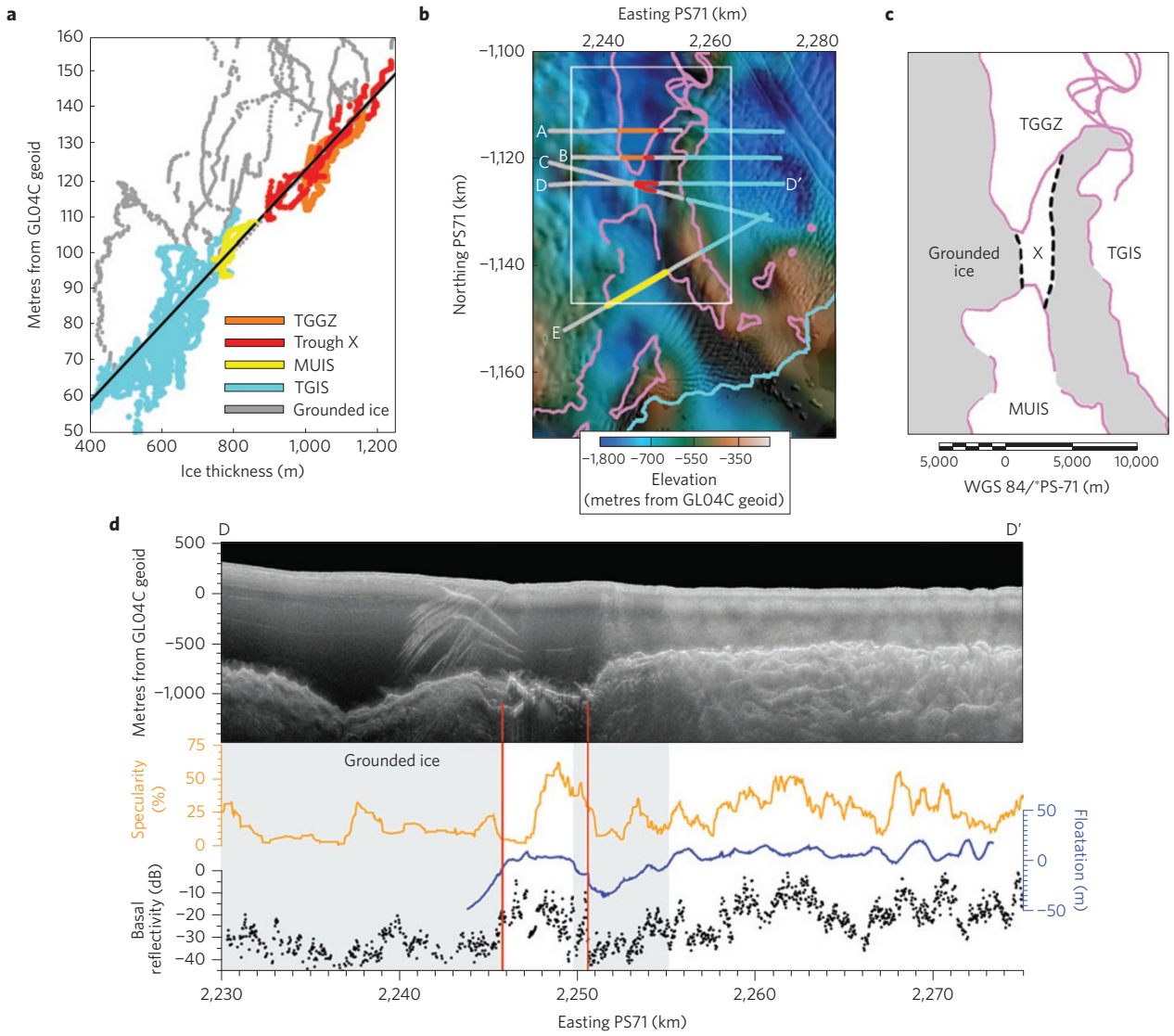

Figure 3 | A newly discovered oceanic entryway to Totten Glacier. a, Ice-surface elevation against ice thickness for the five profiles shown in **b**; the black line represents theoretical floatation. Red points sample the new trough ('Trough X'); yellow, orange and blue points sample previously known floating areas of the MUIS, TGGZ and the TGIS, respectively. **b**, Inverted bathymetry of the northeast area of the TGIS and MOA (ref. 18; partially transparent). **c**, Expanded map of the area outlined in the rectangle in **b** presenting the approximate extent of Trough X (dashed lines). **d**, (Top) Radargram for Profile D–D′. (Bottom) Basal echo strength (black points), hydrostatic anomaly (blue line), and basal specularity (orange line) for Profile D–D′ are shown with the same horizontal scale as the radargram. The proposed extent of Trough X along Profile D–D′ is indicated by the red vertical lines.

smooth the overlying ice, increasing the specularity of the interface. We find high specularity in the trough, extending to the same approximate western extent as the elevated reflectivity, supporting the inference that seawater is found beyond where the ice reaches hydrostatic equilibrium. We find that the ice–water interface in the western half of the trough is more specular than anywhere else along the profile, including the area previously known to be an ice shelf. Combined with hydrostatic equilibrium and elevated basal reflectivity, the high specularity on the western side provides further evidence that smoothing of the interface due to basal melting is underway and that water is present in the trough. Low specularity in the eastern half of the trough indicates a transition in the geometry of the interface, possibly where basal crevasses produce a diffuse scattering environment (Fig. 3).

Based on our analysis of radar data, we suggest the trough width is nearly the same as the half-wavelength of the gravity data and, therefore, near the limit of detectability. This limitation makes a narrow feature difficult to model by inversion as the gravity signal from the two sides is smeared over the trough. However, a short-wavelength gravity low over the trough area (Supplementary Figs 5 and 6) suggests a shallow topographic low where radar results indicate the ice is floating. Simple profile modelling of this gravity line constrained by the radar results implies that the depth of the trough could be as much as 1,400 mbsl, depending on the underlying geology.

Although we are confident in the present floatation of ice over the trough, the question of why this is not reflected in published grounding lines remains. The trough is either undetectable using traditional grounding line mapping methods or floatation occurred recently. The most detailed grounding line for the Sabrina Coast was mapped using tandem double difference interferometry data acquired on the European Remote Sensing (ERS) satellites in 1996 (ref. 14). If the trough is undetectable today, it is even more likely that it was undetectable in 1996 because the ice has thinned substantially since[1,2]. To test this, we model the tidal flexure of the ice over the trough and compare it to what would be detectible with

ERS interferometry. Modelling the ice as a 1,000-m-thick infinite beam[23] with a practical modulus of elasticity from the literature[24] supported by the walls of a water-filled 4.9-km-wide trough, we compute between 39 and 51% of full tidal deflection in the centre of the trough. The published interferogram for the TGIS reveals approximately five double difference fringes for the full range tidal signal[25] indicating that there would be 2 to 2.5 fringes in the centre of the trough. Coherence problems, snowfall, and tropospheric and ionospheric glitches cause noise on the level of a single fringe, making these fringes near the threshold of detectability. The complex fringe patterns in the area lead to discontinuous grounding line recovery and multiple irregular segments[14] (Fig. 3). Even if fringes were detected in the middle of the trough, further interpretation would have been necessary to propose that they are caused by ice floating over a trough. Considering the ice was thicker in 1996 and would have produced an even smaller flexure signal, it is likely that floatation over the trough was not detected at that time.

Warm modified Circumpolar Deep Water (MCDW) observed on the Sabrina Coast continental shelf occupies the bottom layers of the water column, indicating that it will fill deep topography as it flows according to isobaths. This is not the case in most other coastal areas of East Antarctica, where colder, denser Shelf Water occupies the lowest layers[7]. Some have suggested this MCDW could accelerate ice-shelf melting if it enters the TGIS cavity[7,8]; however, until now there was no indication that pathways of sufficient depth existed for it to do so. Previous bathymetry compilations[26,27] interpolate across the TGIS and result in shallow topography that would not allow the observed MCDW to enter the cavity (dashed lines in Fig. 2). As a result, ocean circulation models using these compilations would potentially underestimate heat flux into the cavity. Although a blocking ridge lies beneath the calving front that was possibly a grounding line pinning-point during Holocene retreat of ice, we detect depressions in the ridge deep enough to allow MCDW to enter the cavity.

A previously unknown trough is the deepest entry to the TGIS cavity and well below the range of observed MCDW depths. At nearly 5 km across, the trough is wide enough to affect topographic steering of bottom currents, potentially routing deep layers of MCDW to an area of the coast where we find potential for local marine ice sheet instability landward of the published grounding lines. We speculate that ocean heat flux through the trough contributed to the retreat of the eastern Totten Glacier Grounding Zone (TGGZ; Figs 2 and 3) to its present position, and could contribute to further destabilization of the low-lying area between the TGIS and the similarly deep Reynolds Trough. We estimate that at least 3.5 m of eustatic sea level potential drains through Totten Glacier alone (Supplementary Information), so the area should be monitored for potential perturbations that could result in further retreat.

Although it is possible that the ice over the trough began floating recently, perhaps related to observed regional mass loss acceleration[28] and a 16-year-high TGIS basal melt rate[4] that both occurred in 2006, no early data sets have adequate resolution to test this idea. Considering tidal deflection of the ice over the trough probably went undetected in 1996 and radar surface imagery suggested steep slopes on its sides in 2003, the trough probably predates published grounding lines. In either case, we expect the water column thickness over the trough to increase by several metres per year to maintain hydrostatic equilibrium if thinning trends continue[1,2]. This could allow additional exchange between the TGIS and the ocean, accelerate ice-shelf thinning, and allow grounded ice to accelerate towards the coast. The availability of MCDW and recent accelerated mass loss support the idea that the behaviour of Totten Glacier is an East Antarctic analogue to ocean-driven retreat underway in the West Antarctic Ice Sheet (WAIS). The global sea level potential of 3.5 m flowing through Totten Glacier alone is of similar magnitude to the entire probable contribution of the WAIS (ref. 29). As with the WAIS, much of the broader drainage basin accessible to a retreating Totten Glacier is grounded below sea level, with a potential contribution of 5.1 m (Supplementary Information), so instabilities from ice–ocean interaction in East Antarctica could have significant global consequences.

Methods

Data acquisition. The major source of observational data used herein is the International Collaboration for Exploration of the Cryosphere through Aerogeophysical Profiling (ICECAP) project, which, together with the East Antarctic component of NASA's Operation Ice Bridge mission, acquired the first comprehensive survey of the Aurora Subglacial Basin (ASB; ref. 11) and the Totten Glacier Ice Shelf (TGIS) between 2008 and 2012. The primary data sets used are laser surface altimetry, ice-sounding radar, gravity and magnetics, all acquired with the University of Texas Institute for Geophysics (UTIG) instrumentation suite aboard a ski-equipped BT-67 aircraft. The data were acquired with flights from the Australian Antarctic Division's (AAD) Casey Station. The survey was designed to cross the major axis of the TGIS to highlight channels connecting the inner continental shelf to the ice-shelf cavity. Most profiles are aligned either with the main cavity axis or parallel to the coast where the TGIS turns 20° to the west around the northeast tip of Law Dome (Fig. 1c). Tie lines and other lines of opportunity crossing the cavity were primarily used for levelling, but were included in the compilation to increase data coverage. Detailed line placement was planned to cross the grounding line (including ice rises) to provide areas to judge the quality of subsequent gravity inversions. Gravity data were acquired with a two-axis stabilized gravimeter (Bell Aerospace BGM-3) in the first three years, during which most of the data over the TGIS cavity were obtained. A modern three-axis stabilized gravimeter (Gravimetric Technologies GT-1A) was used in the fourth season to acquire the coast-parallel lines and a few others to fill coverage gaps. The coast-parallel flights were completed as a dedicated gravity survey flying at the minimum practical flight elevation and speed to increase along-track resolution. Scalar magnetic field data were acquired with a Geometrics 823A magnetometer. Meteoric ice thickness and sub-ice reflectivity characteristics were measured using the UTIG coherent, chirped very high frequency radar centred at 60 MHz (ref. 21). Ice-surface altimetry was acquired with a Riegl ice-profiling rangefinder; in addition, a 100-beam photon counting, scanning LiDAR provided ice-surface swath altimetry for approximately 50% of the line km (ref. 30).

Data analysis. Bulk density contrasts were inferred from gravity data using seven 2D profile models in the survey area. The contrasts were interpreted using total magnetic intensity, free air gravity, and depth to magnetic basement grids to infer a suite of possible geologic boundaries and bulk densities that were applied to subsequent 3D bathymetry inversions (Supplementary Information). The inversions were not constrained to areas of known grounded ice so that each result could be compared to known ice-bottom elevations and the quality of the geologic model examined. The root mean square error of the difference between the inverted and known ice-bottom elevations is used in the text as the measure of error in the inversion result. The ice-sounding radar data contains high-frequency information not detectable by airborne gravity, so the RMSE between known and inverted surfaces provides an assessment of the gravity platform's ability to reproduce realistic topography. Gravity data levelling, gridding and inversions were computed using the Geosoft Oasis Montaj software version 8.1, profile and gridded inversions were computed with the Geosoft GMSYS and GMSYS-3D extensions, respectively. Magnetics data were corrected for diurnal variations using static data acquired at Casey Station ~200 km west of the survey area, the large-scale geomagnetic reference field was removed, and the result was then levelled[10]. Depths to magnetic basement solutions were restricted to between 500 m and 10 km from the source to highlight shallow basement sources. The coast-parallel ridge along the TGIS calving front from the gravity inversion corresponds to shallow magnetic depth to basement solutions, consistent with a high-density basement composition with low rates of erosion. Agreement between positive gravity anomalies, shallow magnetic basement, ice rises and grounded icebergs (Supplementary Movies) provides confidence in the geologic model underlying the inversion result. In Fig. 2, thermal forcing was computed as the observed conservative temperature less the *in situ* freezing point for the nearest published conductivity–temperature–depth profiles[7].

Received 12 December 2014; accepted 9 February 2015; published online 16 March 2015

References

1. Flament, T. & Rémy, F. Dynamic thinning of Antarctic glaciers from along-track repeat radar altimetry. *J. Glaciol.* **58,** 830–840 (2012).

2. Pritchard, H. D., Arthern, R. J., Vaughan, D. G. & Edwards, L. A. Extensive dynamic thinning on the margins of the Greenland and Antarctic ice sheets. *Nature* **461,** 971–975 (2009).
3. Pritchard, H. D. *et al.* Antarctic ice-sheet loss driven by basal melting of ice shelves. *Nature* **484,** 502–505 (2012).
4. Gwyther, D. E., Galton-Fenzi, B. K., Hunter, J. R. & Roberts, J. L. Simulated melt rates for the Totten and Dalton ice shelves. *Ocean Sci.* **10,** 267–279 (2014).
5. Khazendar, A. *et al.* Observed thinning of Totten Glacier is linked to coastal polynya variability. *Nature Commun.* **4,** 2857 (2013).
6. Jenkins, A. *et al.* Observations beneath Pine Island Glacier in West Antarctica and implications for its retreat. *Nature Geosci.* **3,** 468–472 (2010).
7. Bindoff, N. L., Rosenberg, M. A. & Warner, M. J. On the circulation and water masses over the Antarctic continental slope and rise between 80 and 150° E. *Deep Sea Res.* **47,** 2299–2326 (2000).
8. Williams, G. D. *et al.* Late winter oceanography off the Sabrina and BANZARE coast (117–128° E), East Antarctica. *Deep Sea Res.* **58,** 1194–1210 (2011).
9. Parker, R. L. The rapid calculation of potential anomalies. *Geophys. J. R. Astron. Soc.* **31,** 447–455 (1973).
10. Aitken, A. R. A. *et al.* The subglacial geology of Wilkes Land, East Antarctica. *Geophys. Res. Lett.* **41,** 2390–2400 (2014).
11. Young, D. A. *et al.* A dynamic early East Antarctic Ice Sheet suggested by ice-covered fjord landscapes. *Nature* **474,** 72–75 (2011).
12. Pollard, D., DeConto, R. M. & Alley, R. B. Potential Antarctic Ice Sheet retreat driven by hydrofracturing and ice cliff failure. *Earth Planet. Sci. Lett.* **412,** 112–121 (2015).
13. Galton-Fenzi, B., Maraldi, C., Coleman, R. & Hunter, J. The cavity under the Amery Ice Shelf, East Antarctica. *J. Glaciol.* **54,** 881–887 (2008).
14. Rignot, E., Mouginot, J. & Scheuchl, B. Antarctic grounding line mapping from differential satellite radar interferometry. *Geophys. Res. Lett.* **38,** L10504 (2011).
15. Bohlander, J. & Scambos, T. *Antarctic Coastlines and Grounding Line Derived from MODIS Mosaic of Antarctica* (*MOA*) (National Snow and Ice Data Center, 2007); http://nsidc.org/data/atlas/news/antarctic_coastlines.html
16. Bindschadler, R., Vaughan, D. G. & Vornberger, P. Variability of basal melt beneath the Pine Island Glacier Ice Shelf, West Antarctica. *J. Glaciol.* **57,** 581–595 (2011).
17. Van den Broeke, M. Depth and density of the Antarctic firn layer. *Arct. Antarct. Alp. Res.* **40,** 432–438 (2008).
18. Scambos, T. A., Haran, T. M., Fahnestock, M. A., Painter, T. H. & Bohlander, J. MODIS-based Mosaic of Antarctica (MOA) data sets: Continent-wide surface morphology and snow grain size. *Remote Sens. Environ.* **111,** 242–257 (2007).
19. Neal, C. Radio echo determination of basal roughness characteristics on the Ross Ice Shelf. *Ann. Glaciol.* **3,** 216–221 (1982).
20. Van Beek, L. Dielectric behaviour of heterogeneous systems. *Prog. Dielectr.* **7,** 69–114 (1967).
21. Peters, M. E., Blankenship, D. D. & Morse, D. L. Analysis techniques for coherent airborne radar sounding: Application to West Antarctic ice streams. *J. Geophys. Res.* **110,** B06303 (2005).
22. Schroeder, D. M., Blankenship, D. D. & Young, D. A. Evidence for a water system transition beneath Thwaites Glacier, West Antarctica. *Proc. Natl Acad. Sci. USA* **110,** 12225–12228 (2013).
23. Holdsworth, G. Flexure of a floating ice tongue. *J. Glaciol.* **8,** 385–397 (1969).
24. Vaughan, D. G. Tidal flexure at ice shelf margins. *J. Geophys. Res.* **100,** 6213–6224 (1995).
25. Rignot, E. Mass balance of East Antarctic glaciers and ice shelves from satellite data. *Ann. Glaciol.* **34,** 217–227 (2002).
26. Fretwell, P. *et al.* Bedmap2: Improved ice bed, surface and thickness datasets for Antarctica. *Cryosphere* **7,** 375–393 (2013).
27. Arndt, J. E. *et al.* The International Bathymetric Chart of the Southern Ocean (IBCSO) Version 1.0—A new bathymetric compilation covering circum-Antarctic waters. *Geophys. Res. Lett.* **40,** 3111–3117 (2013).
28. Chen, J. L., Wilson, C. R., Blankenship, D. & Tapley, B. D. Accelerated Antarctic ice loss from satellite gravity measurements. *Nature Geosci.* **2,** 859–862 (2009).
29. Bamber, J. L., Riva, R. E. M., Vermeersen, B. L. A. & LeBrocq, A. M. Reassessment of the potential sea-level rise from a collapse of the West Antarctic Ice Sheet. *Science* **324,** 901–903 (2009).
30. Young, D. A. *et al.* Land-ice elevation changes from photon-counting swath altimetry: First applications over the Antarctic Ice Sheet. *J. Glaciol.* **61,** 17–28 (2015).

Acknowledgements

This project is the result of the ongoing ICECAP collaboration between the USA, UK and Australia with support from NSF grants PLR-0733025 and PLR-1143843, and CDI-0941678, NASA grants NNG10HPO6C and NNX11AD33G (Operation Ice Bridge and the American Recovery and Reinvestment Act), Australian Antarctic Division projects 3013 and 4077, NERC grant NE/D003733/1, the G. Unger Vetlesen Foundation, the Jackson School of Geosciences, and the Antarctic Climate and Ecosystems Cooperative Research Centre. We thank the captains and crews of Kenn Borek Airlines Ltd, ICECAP project participants, CMG Operations Pty Ltd, and the Geosoft Education Program. We also thank S. Kempf for assistance with radar data processing, as well as A. Leventer, A. Wåhlin, D. Gwyther, K. Soderlund, C. Grima, F. Habbal and S. Zedler for comments on the manuscript. Part of the research was carried out at the Jet Propulsion Laboratory, California Institute of Technology, under a contract with the National Aeronautics and Space Administration. This is UTIG contribution 2831.

Author contributions

J.S.G. performed the gravity inversions, magnetic depth to basement estimates, hydrostatic analysis, applied the bed reflectivity corrections, and wrote the manuscript. D.D.B., D.A.Y. and A.R.A.A. assisted with the potential field interpretations. J.S.G. and T.G.R. performed the initial gravity reduction and J.S.G. levelled the result. J.L.R. estimated the sea level potential for Totten Glacier. B.L. computed the percentage deflection expected for a range of trough widths and commented on what would be detectable using existing ERS data. D.M.S. provided radar technical and interpretation guidance for the discussion of reflectivity and specularity. A.R.A.A. performed the magnetics data reduction. J.L.R., R.C.W. and T.D.v.O. provided the glaciological context for Totten Glacier. J.S.G., D.A.Y., D.D.B., T.D.v.O., J.L.R., M.J.S. and R.C.W. designed the surveys. J.S.G., D.A.Y., T.D.v.O., J.L.R. and R.C.W. collected the data. All authors contributed comments to the interpretation of results and preparation of the final paper.

Additional information

Supplementary information is available in the online version of the paper. Reprints and permissions information is available online at www.nature.com/reprints. Correspondence and requests for materials should be addressed to J.S.G.

Competing financial interests

The authors declare no competing financial interests.